Available online at www.sciencedirect.com
ScienceDirect
Journal of Sound and Vibration 325 (2009) 266–286
JOURNAL OF SOUND AND VIBRATION
www.elsevier.com/locate/jsvi

Structural and acoustic responses of a submarine hull due to propeller forces

Sascha Merz*, Roger Kinns, Nicole Kessissoglou

School of Mechanical and Manufacturing Engineering, University of New South Wales, Sydney, NSW 2052, Australia

Received 20 October 2008; received in revised form 15 December 2008; accepted 7 March 2009
Handling Editor: J. Lam
Available online 15 April 2009

Abstract

The low frequency structural and acoustic responses of a simplified axisymmetric submarine model to fluctuating propeller forces along the submarine axis are investigated. The forces arise from a hydrodynamic mechanism and are transmitted from the propeller to the submarine hull through both the shaft and the fluid. Numerical models have been developed to simulate the strongly coupled structure–fluid interaction of a submerged vessel in the frequency domain. The structure is modelled using the finite element method, so that more complex features such as ring-stiffeners, bulkheads and the propulsion system can be taken into account. A simple, passive vibration attenuation system known as a resonance changer is included in the model of the propeller/shafting system. The surrounding fluid is modelled using the boundary element method. The influence and importance of model parameters such as structural stiffness and fluid loading effects are investigated. Due to the fluctuating propeller forces, the hull is excited by axial structural forces transmitted through the propeller/shafting system as well as by acoustic dipoles, where the dipoles are correlated to the structural forces in strength and direction. The acoustic dipole at the propeller also radiates sound directly to the far field of the surrounding fluid. It is demonstrated that the performance of the RC is negatively influenced at frequencies above the fundamental axial resonance of the hull by the effect of forces transmitted through the fluid. Another problem arises due to increased axial movement of the propeller, when the RC is optimised to minimise excitation of the hull via the propeller shaft. This results in an additional sound field that excites the submarine hull in a similar manner to the fluid forces that arise directly from the hydrodynamic mechanism.

1. Introduction

The reduction of noise emitted by submarines has long been a key topic in naval research. This arises from water being a very good sound transmitter, allowing detection of submarines by passive sonar over large distances [1]. In order to address this problem, the sound sources of a submarine need to be identified. Noise emitted from sources internal to the hull and from the propeller can be distinguished. These internal sources include on-board machinery such as diesel engines and generators, fluid systems and exhaust systems as well as activity by the crew. Propeller noise is attributable to cavitation, flow noise and blade vibration which are

*Corresponding author. Tel.: +61 2 93856864; fax: +61 2 96631222.
E-mail address: sascha.merz@student.unsw.edu.au (S. Merz).

0022-460X/$ - see front matter © 2009 Elsevier Ltd. All rights reserved.
doi:10.1016/j.jsv.2009.03.011

Nomenclature

a	propeller radius
a_f	foundation minor radius
A_0	resonance changer cylinder cross-sectional area
A_1	resonance changer pipe cross-sectional area
A_s	propeller shaft cross-sectional area
b_f	foundation major radius
B	resonance changer oil bulk modulus
$\mathbf{B}_e$	linear operator matrix
c	speed of sound
c_b	shaft bearing damping constant
c_r	resonance changer damping constant
$\mathbf{C}_s$	structural damping matrix
$\mathbf{D}_e$	elemental material matrix
E_f	foundation Young's modulus
E_s	propeller shaft Young's modulus
f	force
f_h	hull drive point force
f_p	propeller force
$\mathbf{f}_s$	structural load vector of nodal forces
$g(r)$	Green's function
$\mathbf{G}$	BEM double layer influence matrix
h_f	foundation shell thickness
$\mathbf{H}$	BEM single layer influence matrix
i	index
k	wavenumber
k_b	shaft bearing spring constant
k_r	resonance changer stiffness constant
$\mathbf{K}_s$	structural stiffness matrix
l_s	overall propeller shaft length
l_{se}	effective propeller shaft length
L	resonance changer pipe length
m_b	shaft bearing mass
m_p	propeller mass
m_{pf}	propeller added mass of water
m_r	resonance changer mass
$\mathbf{M}_s$	structural mass matrix
$\mathbf{n}$	surface normal vector
$\mathbf{N}$	matrix of interpolation functions
$\mathbf{p}$	vector of nodal pressures
P	pressure in time domain
p	pressure
$\mathbf{p}_{\text{inc}}$	vector of nodal pressures for the undisturbed incident field
r	radial coordinate
r_a	normalised radiation resistance of the propeller
r_i	nodal radial coordinate
$\mathbf{R}_{fs}$	coupling matrix, relating displacement degrees of freedom to normal velocity degrees of freedom
$\mathbf{R}_{sf}$	coupling matrix, relating pressure degrees of freedom to nodal forces
t	time
t_i	nodal shell thickness
$\mathbf{u}$	vector of nodal displacements
u	radial displacement
u_i	nodal shell radial displacement
v_h	hull drive point velocity
$\mathbf{v}_n$	vector of nodal surface normal velocities
v_n	velocity in surface normal direction
v_p	propeller axial velocity
w	axial displacement
w_i	nodal shell axial displacement
x_a	normalised radiation reactance of the propeller
z	axial coordinate
z_a	normalised radiation impedance of the propeller
z_c	characteristic impedance of the fluid
z_i	nodal axial coordinate
α_i	nodal shell surface angle
Γ_{int}	structure/fluid interaction surface
Γ_p	surface of an element at the structure/fluid interface
ζ_e	damping ratio for an element
η	local shell coordinate in surface normal direction
θ	circumferential coordinate, directional angle for dipole
λ	wavelength
μ	resonance changer oil dynamic viscosity
ν_f	foundation Poisson's ratio
ξ	local shell coordinate along surface
ρ	density of the fluid
ρ_e	material density for an element
ρ_f	foundation density
ρ_r	resonance changer oil density
ρ_s	propeller shaft density
ϕ_i	nodal shell rotation
ω	circular frequency
Ω_e	structural domain for an element

strongly influenced by spatial and temporal variations of velocity in the wake [2,3] as well as by the rotation of blade thickness and thrust. Since submarines usually operate at large depths, cavitation is suppressed by the high water pressure. Propeller blades are sickle shaped to reduce net fluctuating forces due to imperfections in the incident wake field. Flow noise is moderated by travelling at low speeds. The overall sound signature is a combination of tonals and broadband random noise. The prevalence of the sound sources depends on the frequency band, speed and depth. At large distances from the hull, the lower frequencies dominate since absorption increases with frequency. Tonal components are more distinctive than random noise, but the combination of tonal components at different frequencies with broadband noise provides important information about the identity and speed of the submarine. At higher speeds in particular, the propeller is the most significant source of tonal and broadband noise.

The operation of the propeller in a non-uniform wake, as shown in Fig. 1, is the most important reason for the generation of tonal noise. The non-uniformity of the wake is due to asymmetry in the hull or protrusions of control surfaces, as shown in Fig. 2 [4]. As the propeller blades rotate through areas of different water velocity, fluctuations in thrust are generated at the blade-passing frequency (number of blades multiplied by the propeller rotational speed) and its multiples. Fluctuating forces of similar order also arise in the vertical and transverse directions. The observed tonal components arise primarily from this spatial variation in the wake field, combined with the usually smaller effects of the rotation of blade thrust and blade thickness. These tonal components are complemented by random components due to turbulence in the wake flow at entry to the propeller and also turbulence generated by flow over the blades. The variation in thrust causes structural excitation of the hull through the propeller/shafting system, resulting in vibration of the hull and the propeller. The low frequency vibrational modes of the hull and propeller/shafting system can result in a high level of radiated noise [5]. In addition, the same hydrodynamic mechanism results in dipole sound radiation at the propeller, where the dipoles can be correlated to the structural forces in strength and direction. The dipole sound radiation of the propeller also contributes to excitation of the hull, via the combination of the hydrodynamic near field and the acoustic far field. The pressure field in the immediate vicinity of the propeller

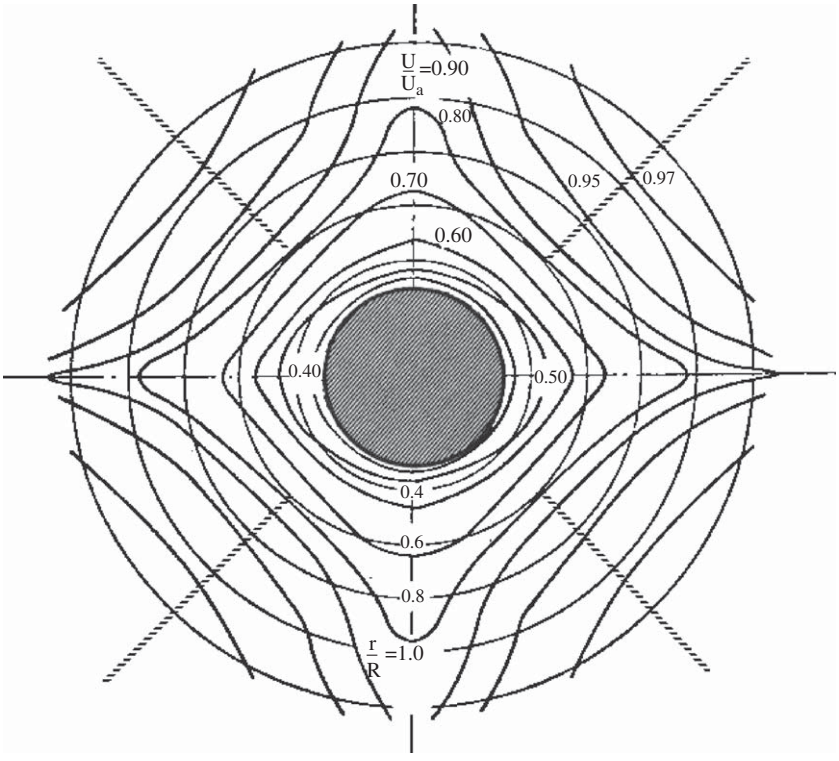

Fig. 1. Wake of a torpedo [1].

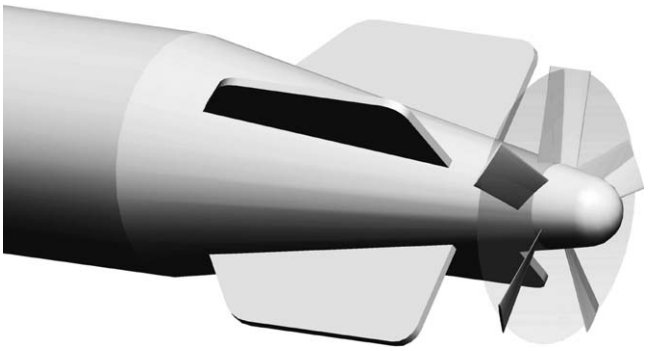

Fig. 2. Stern of a torpedo.

is highly complex [6]; it reflects the distribution and variation with time of fluctuating forces over the whole of the propeller disc. The nature of this pressure field is described by Breslin and Anderson [7], who show how many components decay rapidly with distance, leaving a simpler field with well-defined characteristics further from the propeller. These rapidly decaying components include the effects of rotating forces and blade volumes that are not associated with a net fluctuating shaft force [8]. The acoustic fields of the rapidly decaying components are usually weak in relation to other components. In the absence of cavitation, the net fluctuating forces on the propeller tend to govern the field at more than a few diameters from the propeller. This field has the characteristics associated with acoustic dipoles in the axial and radial directions [9]. Each has a near field, decaying as $1/r^2$, and an acoustic far field, decaying as $1/r$. The transition between the near and far-field components occurs within a few propeller diameters at frequencies of interest, becoming closer to the propeller as frequency increases. Simplification to a combination of axial thrust and the associated axial dipole allows fundamental aspects of the problem to be explored and understood; both have the potential to excite breathing modes of an axisymmetric hull. It also avoids the need to specify details of a propeller design and wake field that would be required to define the complete pressure field.

As a simplification, the propeller and shaft might be envisaged as a spring–mass system having one natural frequency, where the propeller is the mass and the shaft is the spring. In reality, the propeller/shafting system is more complicated as there are other components such as the thrust bearing and foundation that contribute to its overall dynamic behaviour. These features are included in the model described in this paper. However, in the low frequency range only the fundamental frequency is of importance. Since the shaft passes through the tailcone, it is comparatively long and flexible. This leads to a low fundamental resonant frequency of the propeller/shafting system, involving significant axial vibration at its fundamental resonant frequency. Consequently, the propeller/shafting system can cause significant axial vibration of the pressure hull and sound radiation, even at a frequency that does not match one of the natural frequencies of the hull [5].

At low frequencies, the pressure hull can be represented by a thin-walled cylinder reinforced by ring-stiffeners and bulkheads to withstand hydrostatic pressure at large depths. The pressure hull end closures are typically flat or hemispherical. Changes in hydrodynamic pressure do not cause the overall dynamic behaviour to change markedly at operational depths [10]. The thrust block is close to the stern end plate. For this reason, vibration of the hull can be excited through the propeller/shafting system that is correlated to the bending and accordion modes of a free thin-walled cylindrical shell. Vibration correlated to the accordion modes is known to be an effective sound radiator, whilst vibration correlated to the bending modes is usually less effective.

To attenuate axial vibration of the propeller/shafting system and thereby reduce the transmission of axial forces from the propeller to the hull, a device known as a resonance changer (RC) can be implemented in the propeller/shafting system. The RC, initially derived from a thrust-meter, is a hydraulic vibration absorber that can be represented by a virtual spring–mass–damper system [11]. It detunes the natural frequencies of the propeller/shafting system and introduces additional damping.

Early models to find optimal RC parameters treated the submarine hull as a rigid termination [11] or one-dimensional rod model [12]. In recent work, a simplified physical model of a submarine was included to consider the hull impedance, hull resonances and radiated sound due to shaft excitation [5]. Results were also

obtained for a series of RCs with variable parameters. However, the excitation of the submarine hull from the dipole field radiated by the propeller has not been considered in this context. It was assumed previously that the dipole excitation is negligible, as earlier research predicted a contribution that is only 6–8 percent of the contribution of the structural force, where the Laplace equation was used to model the fluid [13]. Recent work using the Helmholtz equation has shown that the contribution of fluid forces to the overall excitation can be between 10 and 50 percent of the response due to excitation through the shaft [14,15]. This is because the transition from the hydrodynamic near field to the acoustic far field occurs close to the propeller at frequencies of practical interest. Another problem arising from the use of an RC to minimise excitation of a submarine hull is that the axial movement of the propeller can be increased [5]. This causes additional sound radiation from the propeller.

The dynamic behaviour of the free-flooded tailcone that supports the aftmost propeller bearing is of particular interest. Pan et al. [16] used a simplified analytical representation of this cone to show that it could have a major effect on sound radiation due to an axial force applied at the propeller thrust bearing, depending on assumed boundary conditions for the cone. The fluid forces were not considered in Ref. [16], but the excitation of the tailcone by the pressure field near the propeller further increases the potential significance of tailcone characteristics. For this reason, the dynamic behaviour of the cone has been explored in this work, using various assumptions concerning cone stiffness and internal water loading.

In this paper, numerical models have been developed to simulate the strongly coupled fluid–structure interaction of a submerged vessel at low frequencies. The hull is considered to be under both structural and acoustic excitation from the propeller. The effect of the tailcone on the hull excitation and dynamic response is presented. The performance of an RC implemented in a propeller–shafting system to attenuate axial forces from the propeller to the hull, in the presence of dipole excitation of the hull surfaces, is investigated. Furthermore, the magnitude of additional sound radiation from the propeller due to its increased axial vibration induced by the RC is examined.

For all models, the finite element method (FEM) [17,18] was used to model the structure and the direct boundary element method (DBEM) [19] was used to model the fluid domain. The FEM software package ANSYS 11 was utilised to generate the structural stiffness, damping and mass matrices and the meshes. Software developed by the first author was used to compute the structure/fluid coupling matrices as well as the DBEM matrices. Sparse direct equation solvers from the scientific software suite SciPy were then used to solve the coupled system of equations.

2. Dynamic model of the submarine

Only axial excitation of the submarine hull has been considered in this work as the accordion modes are particularly effective sound radiators. An axisymmetric model was used. The model consists of two parts, the propeller/shafting system and the submarine hull.

A real submarine has the pressure hull as its main structure with external attachments, such as buoyancy tanks that are of relatively light construction. The pressure hull, depicted in Fig. 3, has been shown to control hull dynamic properties at low frequencies [20]. The pressure hull was modelled as a thin-walled cylinder with evenly spaced ring-stiffeners of rectangular cross-section. In addition, two evenly spaced bulkheads were included in the model as circular plates. The end plates of the pressure hull have been treated as rigid as they are relatively stiff. The on-board machinery and remaining internal structure were considered as a distributed mass of the cylindrical shell. The distributed mass was chosen in such a way that neutral buoyancy of the submarine is guaranteed [5]. Lumped masses were added to both end plates to represent the water in ballast

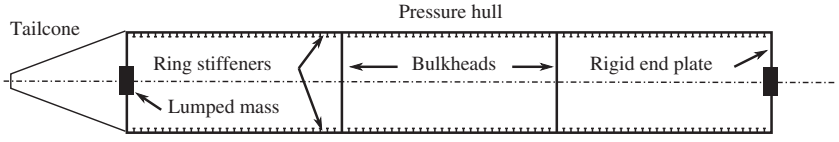

Fig. 3. Simplified physical model of the submarine hull.

tanks and free-flooded structures. The elongated tailcone was considered explicitly since the dipole excitation of the hull originates at the propeller hub.

The basic elements of the propeller/shafting system relevant for axisymmetric analysis are the propeller, shaft, thrust bearing, RC and foundation, as shown in Fig. 4. A modular approach for the propeller/shafting system is shown in Fig. 5, where the propeller force and velocity amplitude are given by f_p and v_p, respectively. The hull drive point force and velocity are denoted by f_h and v_h. The propeller is represented by a lumped mass m_p that also includes the added mass effect of the water. The propeller dimensions for calculating the propeller mass and the added mass of water effect are chosen by assuming that the propeller volume is $\frac{1}{1000}$ of the volume displaced by the pressure hull. The propeller diameter is assumed to be half the pressure hull diameter. The propeller shaft was modelled as a simple rod with an effective length l_{se} and an overall length l_s, where the overhang was represented by another lumped mass. The shaft properties are also defined by its cross-sectional area A_s, Young's modulus E_s and density ρ_s. The thrust bearing was assumed to act as a spring–mass–damper system with mass m_b, damping coefficient c_b and spring constant k_b. For the present model, the thrust bearing is attached to a single RC that has been reduced to a spring–mass–damper system according to Goodwin [11]. The RC incorporates a hydraulic cylinder that is connected to a reservoir via a pipe, as shown in Fig. 6. Virtual mass, damping and stiffness are calculated using [11]

$$m_r = \frac{\rho_r A_0^2 L}{A_1}; \quad c_r = 8\pi\mu L \frac{A_0^2}{A_1^2}; \quad k_r = \frac{A_0^2 B}{V}, \tag{1}$$

where ρ_r is the density of the hydraulic medium, μ is the dynamic viscosity and B is the bulk modulus of the oil in the RC. V is the volume of the reservoir, A_1 is the cross-sectional area of the pipe, L is the pipe length and A_0 is the cross-sectional area of the cylinder.

In a real submarine, the foundation of the propeller/shafting system is a complex shell-like structure, but here it is represented as a truncated cone for the axisymmetric model with end radii a_f and b_f. The Young's modulus, density, Poisson's ratio and thickness of the foundation are given by E_f, ρ_f, v_f and h_f, respectively.

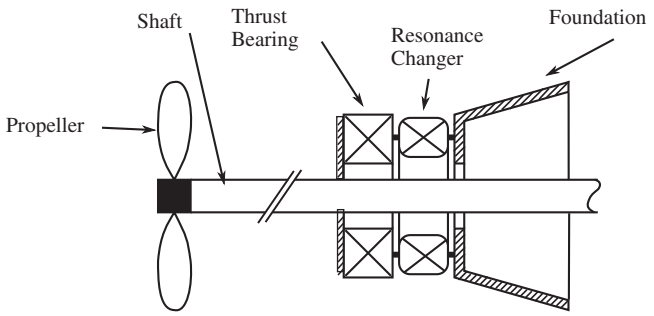

Fig. 4. Propeller/shafting system.

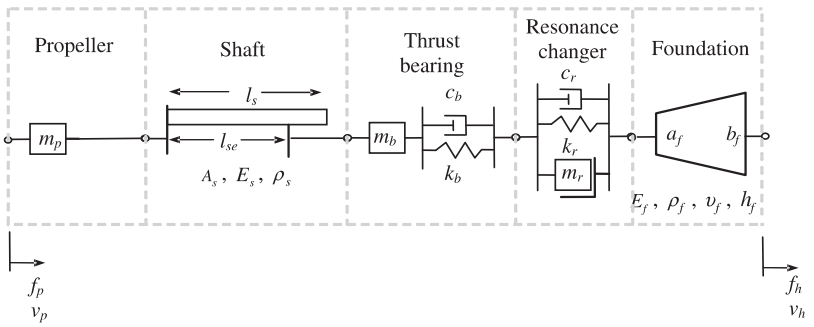

Fig. 5. Simplified physical model of the propeller/shafting system.

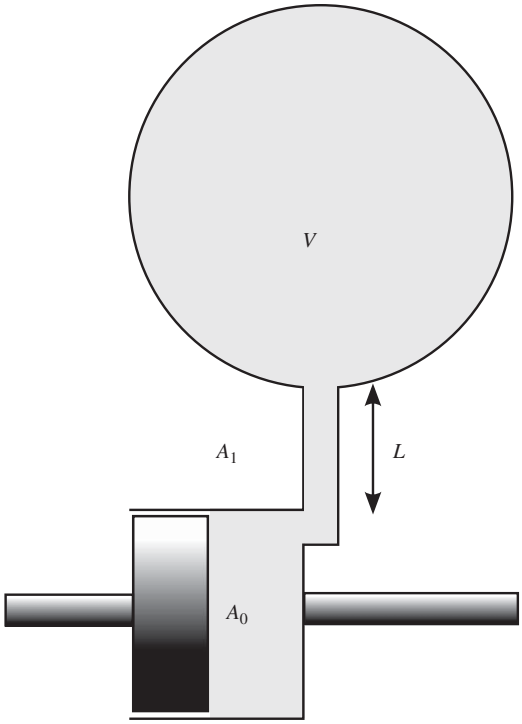

Fig. 6. Resonance changer.

3. Formulation of the problem

The given problem is a classic fluid/structure interaction problem with strong coupling due to the similar densities of fluid and structure. It also includes sound radiation and scattering due to structural vibration and acoustic sources. Furthermore, it can be characterised by sound radiation into an unbounded domain which requires the Sommerfeld radiation condition to be satisfied. Vibration is assumed to be harmonic and linear. Spectral analysis allows broadband random excitation to be taken into account. Therefore the analysis can be conducted in the frequency domain and all displacements, pressures and velocities are represented by their complex amplitude. The time dependence $e^{j\omega t}$ has been omitted, if not stated otherwise.

The problem consists of the structural part and the acoustic part. For the structural part, the FEM was utilised. For the acoustic part, the DBEM was used. For each case, the field variables are described for each element and have to be coupled at the structure/fluid interface. This can be done using the linearised momentum equation, where the surface normal velocity of the structure can be related to the surface pressure gradient by

$$\frac{\partial p}{\partial n} = -j\omega\rho v_n, \tag{2}$$

where p is the acoustic pressure, $\mathbf{n}$ is the surface normal vector, ρ is the density of the fluid and v_n is the velocity component normal to the surface. The discrete systems for both the structural and acoustic parts must be expressed in terms of the structural displacement and acoustic pressure, respectively.

3.1. FE modelling

The structure that interacts with the fluid is represented by a thin-walled axisymmetric shell of finite elements based on Reissner–Mindlin theory, where transverse shear deformation is allowed. The stress component normal to the shell is assumed to be zero throughout the shell thickness. The global strains can

then be expressed as [21]

$$\boldsymbol{\varepsilon} = \begin{Bmatrix} \varepsilon_r \\ \varepsilon_z \\ \varepsilon_\theta \\ \gamma_{rz} \end{Bmatrix} = \begin{Bmatrix} \mathrm{d}u/\mathrm{d}r \\ \mathrm{d}w/\mathrm{d}z \\ u/r \\ \mathrm{d}u/\mathrm{d}z + \mathrm{d}w/\mathrm{d}r \end{Bmatrix}, \tag{3}$$

where 'r' denotes the radial direction, 'z' the axial direction and 'θ' the circumferential direction. Furthermore, u and w are the global radial and axial displacements, respectively. Rod, mass and spring–damper elements have been used in the analysis for the internal structure of the submarine hull and for the propeller/shafting system.

Applying the principle of virtual displacements, a finite element formulation for the structural part of the dynamic problem can be written as

$$\delta\mathbf{u}^{\mathrm{T}} \sum_e \int_{\Omega_e} \mathbf{B}_e^{\mathrm{T}} \mathbf{D}_e \mathbf{B}_e \,\mathrm{d}\Omega_e \mathbf{u} = \delta\mathbf{u}^{\mathrm{T}} \left(-\sum_e \rho_e \int_{\Omega_e} \mathbf{N}_s^{\mathrm{T}} \mathbf{N}_s \,\mathrm{d}\Omega_e \ddot{\mathbf{u}} - \sum_e \zeta_e \int_{\Omega_e} \mathbf{B}_e^{\mathrm{T}} \mathbf{D}_e \mathbf{B}_e \,\mathrm{d}\Omega_e \dot{\mathbf{u}} - \sum_e \int_{\Gamma_p} \mathbf{N}_s^{\mathrm{T}} \mathbf{n} \mathbf{N}_f \,\mathrm{d}\Gamma_p \mathbf{p} + \mathbf{f}_s \right), \tag{4}$$

where 'e' denotes an element, $\mathbf{u}$ is the vector of nodal displacements, $\delta\mathbf{u}$ is a vector of virtual displacements and $\mathbf{p}$ is the vector of nodal pressures at the structure/fluid interface. Ω_e is the structure domain for an element and Γ_p is the surface of an element at the structure/fluid interface. $\mathbf{B}_e$ is a linear operator matrix that relates strain to nodal displacements, $\mathbf{D}_e$ is the elemental material matrix and $\mathbf{N}$ are matrices of interpolation functions, where 's' denotes structural and 'f' denotes acoustic fluid elements. ρ_e is the material density for the element, ζ_e the damping ratio for the element and $\mathbf{f}_s$ is the structural load vector of nodal forces.

By assuming that all $\delta u_i = 1$ for each degree of freedom i and as the displacements are time-harmonic, Eq. (4) can be rewritten as

$$[\mathbf{K}_s + \mathrm{j}\omega\mathbf{C}_s - \omega^2\mathbf{M}_s]\mathbf{u} + \mathbf{R}_{sf}\mathbf{p} = \mathbf{f}_s, \tag{5}$$

where $\mathbf{K}_s$, $\mathbf{C}_s$ and $\mathbf{M}_s$ are the structural stiffness, damping and mass matrices, respectively. $\mathbf{R}_{sf}$ is the matrix that couples pressure degrees of freedom to nodal forces.

For the shell structure, quadratic elements have been used. The displacement variables are interpolated as

$$u = \sum_{i=1}^{3} N_i \left[u_i - \frac{1}{2}\eta t_i \sin(\alpha_i)\phi_i \right], \tag{6}$$

$$w = \sum_{i=1}^{3} N_i \left[w_i + \frac{1}{2}\eta t_i \cos(\alpha_i)\phi_i \right], \tag{7}$$

where the t_i, u_i, w_i, α_i ϕ_i are the thickness, radial displacement, axial displacement, shell surface angle and rotation in the nodes, respectively, and i denotes the element node. The local coordinate in the direction normal to the shell is denoted by η. The shape functions are given by

$$N_1 = \tfrac{1}{2}(\xi^2 - \xi); \quad N_2 = \tfrac{1}{2}(\xi^2 + \xi); \quad N_3 = 1 - \xi^2, \tag{8}$$

where ξ is the local coordinate along the shell surface.

The geometric variables corresponding to the radial and axial location of the shell element are interpolated as

$$r = \sum_{i=1}^{3} N_i \left[r_i + \frac{1}{2}\eta t_i \cos(\alpha_i) \right], \tag{9}$$

$$z = \sum_{i=1}^{3} N_i \left[z_i + \frac{1}{2} \eta t_i \sin(\alpha_i) \right], \tag{10}$$

where r_i and z_i are the nodal radial and axial coordinates. The angles α_i can be found by setting η to zero.

3.2. BE modelling

The fluid domains are described by the linearised wave equation for small amplitudes:

$$\Delta P - \frac{1}{c^2} \frac{\partial^2 P}{\partial t^2} = 0, \tag{11}$$

where P is the acoustic pressure and c is the speed of sound. By assuming time-harmonic waves, the acoustic pressure P fluctuates sinusoidally with the angular frequency ω so that $P = p\,\mathrm{e}^{\mathrm{j}\omega t}$. Here p is the complex amplitude of the pressure fluctuations. For a homogeneous fluid, Eq. (11) becomes

$$\Delta p + k^2 p = 0, \tag{12}$$

where $k = \omega/c$ is the wavenumber. Application of the Green theorem leads to the Kirchhoff–Helmholtz equation, on which the direct boundary element method (DBEM) is based. It relates the field pressure to the surface pressure of an oscillating structure by [22]

$$p(r) = \int_{\Gamma_p} \left(g(r) \frac{\partial p}{\partial n} - p \frac{\partial g(r)}{\partial n} \right) \mathrm{d}\Gamma_p, \tag{13}$$

where $g(r) = \mathrm{e}^{-\mathrm{j}kr}/4\pi r$ is the free space Green's function and the surface normal vector points into the fluid domain. Using Eq. (2) and moving the field point to the surface, Eq. (13) becomes

$$c(r)p(r) = -\int_{\Gamma_p} \left(\mathrm{j}\rho\omega v_n g(r) + p \frac{\partial g(r)}{\partial n} \right) \mathrm{d}\Gamma_p, \tag{14}$$

where

$$c(r) = 1 - \int_{\Gamma_p} \frac{\partial g_0(r)}{\partial n}\, \mathrm{d}\Gamma_p \tag{15}$$

for an exterior problem and

$$c(r) = \int_{\Gamma_p} \frac{\partial g_0(r)}{\partial n}\, \mathrm{d}\Gamma_p \tag{16}$$

for an interior problem, where $g_0(r) = 1/4\pi r$.

It can be shown that in the presence of an incident field, for an exterior problem, Eq. (14) becomes [23]

$$c(r)p(r) = -\int_{\Gamma_p} \left(\mathrm{j}\rho\omega v_n g(r) + p \frac{\partial g(r)}{\partial n} \right) \mathrm{d}\Gamma_p + p_{\mathrm{inc}}(r), \tag{17}$$

where $p_{\mathrm{inc}}(r)$ is the incident field, for example due to an acoustic dipole. The boundary $\mathrm{d}\Gamma_p$ can be subdivided into elements. When using linear isoparametric elements, the pressure and normal velocity can be collocated at the elemental nodes. The interpolation functions for the geometry and boundary variables are then given by

$$N_1 = \tfrac{1}{2}(1 - \xi); \quad N_2 = \tfrac{1}{2}(1 + \xi). \tag{18}$$

Numerical integration can be conducted for each element by using an elliptic integral formulation [24]. This results in the system of equations

$$\mathbf{G}\mathbf{v}_n + \mathbf{H}\mathbf{p} = \mathbf{p}_{\mathrm{inc}}, \tag{19}$$

where $\mathbf{G}$ and $\mathbf{H}$ are the DBEM influence matrices, $\mathbf{v}_n$ is the vector of nodal surface normal velocities, $\mathbf{p}$ is the vector of nodal pressures and $\mathbf{p}_{\mathrm{inc}}$ is the vector of nodal pressures for the undisturbed incident field.

3.3. FE/BE coupling

As the density of the fluid is similar to that of the structure, strong coupling has to be considered. Rewriting Eq. (5) by considering internal and external structure/fluid interaction surfaces separately yields

$$[\mathbf{K}_s + \mathrm{j}\omega\mathbf{C}_s - \omega^2\mathbf{M}_s]\mathbf{u} + \mathbf{R}_{sf,\mathrm{in}}\mathbf{p}_{\mathrm{in}} + \mathbf{R}_{sf,\mathrm{ex}}\mathbf{p}_{\mathrm{ex}} = \mathbf{f}_s, \tag{20}$$

where 'in' and 'ex' denote the internal and external fluid domains, respectively. Eq. (19) can be rewritten as

$$\mathbf{G}_{\mathrm{in}}\mathbf{R}_{fs,\mathrm{in}}\mathbf{u} + \mathbf{H}_{\mathrm{in}}\mathbf{p}_{\mathrm{in}} = \mathbf{0} \tag{21}$$

for the internal problem and

$$\mathbf{G}_{\mathrm{ex}}\mathbf{R}_{fs,\mathrm{ex}}\mathbf{u} + \mathbf{H}_{\mathrm{ex}}\mathbf{p}_{\mathrm{ex}} = \mathbf{p}_{\mathrm{inc}} \tag{22}$$

for the external problem. Eqs. (20)–(22) can be combined to a coupled system of equations

$$\begin{bmatrix} \mathbf{K}_s + \mathrm{j}\omega\mathbf{C}_s - \omega^2\mathbf{M}_s & \mathbf{R}_{sf,\mathrm{ex}} & \mathbf{R}_{sf,\mathrm{in}} \\ \mathbf{G}_{\mathrm{ex}}\mathbf{R}_{fs,\mathrm{ex}} & \mathbf{H}_{\mathrm{ex}} & \mathbf{0} \\ \mathbf{G}_{\mathrm{in}}\mathbf{R}_{fs,\mathrm{in}} & \mathbf{0} & \mathbf{H}_{\mathrm{in}} \end{bmatrix} \begin{Bmatrix} \mathbf{u} \\ \mathbf{p}_{\mathrm{ex}} \\ \mathbf{p}_{\mathrm{in}} \end{Bmatrix} = \begin{Bmatrix} \mathbf{f}_s \\ \mathbf{p}_{\mathrm{inc}} \\ \mathbf{0} \end{Bmatrix}. \tag{23}$$

The coupling matrices are generated by averaging the degrees of freedom of the structural and acoustic domains over the interaction surfaces Γ_{int} [25]. The structure/fluid coupling matrices are then obtained by

$$\mathbf{R}_{sf} = \int_{\Gamma_{\mathrm{int}}} \mathbf{N}_s^{\mathrm{T}}\mathbf{n}\mathbf{N}_f \,\mathrm{d}\Gamma_{\mathrm{int}}, \tag{24}$$

where $\mathbf{N}_s$ and $\mathbf{N}_f$ are the global interpolation functions for the structural and fluid domains, respectively, and $\mathbf{n}$ is the surface normal vector. As an approximation, the shape function for the structural elements is evaluated at the mid-surface as the thickness of the shell is small compared to the wave length. The fluid/structure coupling matrices are obtained by

$$\mathbf{R}_{fs} = \mathrm{j}\omega\mathbf{S}^{-1}\mathbf{R}_{sf}^{\mathrm{T}}, \tag{25}$$

where

$$\mathbf{S} = \int_{\Gamma_{\mathrm{int}}} \mathbf{N}_f^{\mathrm{T}}\mathbf{N}_f \,\mathrm{d}\Gamma_{\mathrm{int}}. \tag{26}$$

4. Sound field radiated by the propeller

The sound field radiated from the propeller is due to (i) the hydrodynamic mechanism that arises through the propeller operating in a non-uniform wake and (ii) the axial fluctuation of the propeller due to vibration of the shafting system. The sound radiation originates from the propeller blades as multiple dipoles. The dipoles can be simplified to a single dipole located at the propeller hub, because the wavelength is large relative to the propeller diameter and the propeller is small relative to the submarine. A derivation of the dipole field pressure due to a fluctuating force is provided by Ross [1]. The directivity pattern of the dipole is governed by $\cos\theta$, where θ is the angle between the field point vector with respect to the source and the force direction. The amplitude is directly proportional to the structural force. The radial variation of the amplitude follows $1/r^2$ in the near field and $1/r$ in the far field, where r is the distance of the field point from the source. The transition is a function of the wavelength λ and occurs at $\lambda/2\pi$. A polar diagram of a dipole is given in Fig. 7.

For (i), the sound radiation due to the force on the propeller hub is

$$p(r,\theta) = \mathrm{j}kfg(r)\left(1 - \frac{j}{kr}\right)\cos\theta, \tag{27}$$

where k is the wavenumber, $g(r)$ is the free space Green's function and f is the amplitude of the exciting force.

For (ii), the propeller was simplified as a rigid circular disc. The problem reduces to a dipole according to Eq. (27) for values of $ka<0.5$, where a is the disc radius. The velocity v_p of the propeller can be related to the

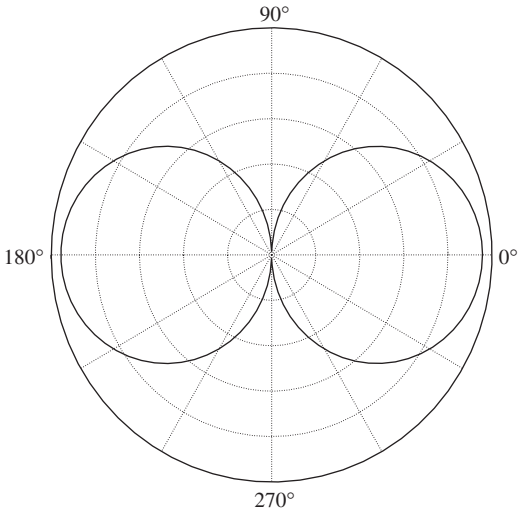

Fig. 7. Dipole directivity pattern.

equivalent force by

$$f = 2sz_c z_a v_p, \tag{28}$$

where $s = \pi a^2$ is the area of a disc surface, z_c is the characteristic impedance of the fluid and $z_a = r_a + \mathrm{j}x_a$, where

$$r_a = \frac{8(ka)^4}{27\pi^2} \quad \text{and} \quad x_a = \frac{4ka}{3\pi} \tag{29}$$

are, respectively, the normalised radiation resistance and reactance. The added mass of water for the propeller due to fluid loading can be found using Eqs. (28) and (29) and is given by

$$m_{pf} = \tfrac{8}{3}a^3\rho, \tag{30}$$

where ρ is the density of the fluid. The radiation damping due to fluid loading is negligible for the model presented here.

5. Results

Fully coupled models have been developed in this work where the structural domain is represented by finite elements and the exterior and interior fluid domains are represented by boundary elements. The FE matrices and all meshes were generated by ANSYS 11. The BE and coupling matrices have been computed with a software implemented in SciPy and C++. The coupled system of equations was solved using SciPy routines. The FE mesh for the submarine hull and the BE meshes are given in Figs. 8 and 9. Fig. 8(a) shows a detail of the FE mesh at the cone and Fig. 8(b) shows a detail of the FE mesh at a bulkhead. Other parts of the mesh have a similar structure. The end plate is rigid, so its grid resolution has no influence on the results. As the joints, especially at the bulkheads and end plates, lead to evanescent near-field waves with a small wavelength, a fine FE mesh is required for convergence of the results in terms of the natural frequencies and displacements.

It is investigated whether the free flooded tailcone can be simplified to a rigid cone, where the internal water is represented by a lumped mass, without significantly changing the dynamic and acoustic behaviour of the submarine. For the models where the internal fluid of the cone was simplified to a lumped mass, a two-field problem was formulated and convergence could be achieved with a grid as shown in Fig. 9(a). In this case, there are at least 20 elements per fluid wavelength present. For the models where the cone internal fluid was modelled using boundary elements, a three-field problem was formulated and a much smaller element size was required to achieve convergence. The mesh for the cone internal fluid is shown in Fig. 9(b). Note that the same

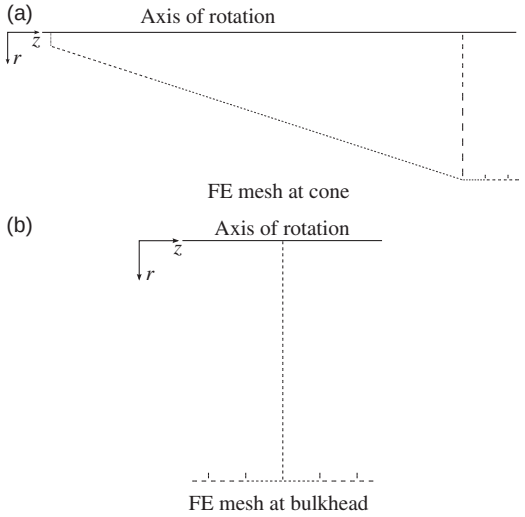

Fig. 8. FE meshes, where r is the radial direction and z is the axial direction. The generators of the axisymmetric elements are depictured as lines. The lines are swept around the axis of rotation and form thin walled rings, frustra or annuli, depending on the orientation.

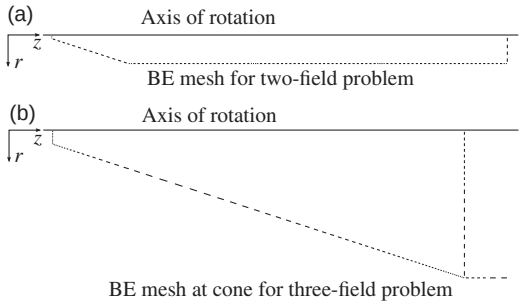

Fig. 9. BE meshes, where r is the radial direction and z is the axial direction. As for the FE meshes, the generators of the axisymmetric elements are depicted as lines.

element size has been used for the exterior fluid domain at the cone for the three-field model. The model parameters are given in Tables 1 and 2 for the propeller/shafting system and the submarine hull, respectively.

5.1. Dynamic behaviour of the propeller/shafting system

The dynamic response of the propeller/shafting system has been investigated with emphasis on the force transmissibility and the propeller vibration, with and without an RC. The axial force on the propeller is proportional to the square of propeller rotational frequency. In Ref. [12], the maximum of the ω^2-weighted force transmissibility in the frequency range of interest was considered as the cost function when optimising the RC parameters for a simplified submarine/propulsion system model of dimensions similar to the models in this work. Optimisation of the weighted force transmissibility was chosen under the assumption that it corresponds to the radiated sound power from the hull. Due to the frequency weighting, lower force transmissibility of the optimised system is expected at the higher frequency range. However, in Ref. [12], acoustic excitation of the submarine hull was not taken into account for the optimisation. The RC parameters from Ref. [12] have also been employed in this work.

The drive point impedance has been examined in order to investigate its influence on the force transmissibility of the propeller/shafting system. The force transmissibility of the structurally excited propeller/shafting system with a rigid termination is compared to the force transmissibility of the propeller/shafting system that is coupled to the simplified physical model of the fluid loaded submarine hull. The results

Table 1
Propeller/shafting system data.

Parameter	Value	Unit
Propeller structural mass	10,000	kg
Propeller added mass of water	11,443	kg
Shaft Young's modulus	200	GPa
Shaft Poisson's ratio	0.3	
Shaft density	7800	kg/m^3
Shaft cross-sectional area	0.071	m^2
Shaft length	10.5	m
Effective shaft length	9	m
Bearing mass	200	kg
Bearing stiffness	20,000	MN/m
Bearing damping	300,000	kg/s
Resonance changer mass	1000	kg
Resonance changer stiffness	169	MN/m
Resonance changer damping	287×10^3	kg/s
Foundation major radius	1.25	m
Foundation minor radius	0.52	m
Foundation half angle	15	deg
Foundation thickness	10	mm
Foundation Young's modulus	200	GPa
Foundation density	7800	kg/m^3

Table 2
Hull data.

Parameter	Value	Unit
Cylinder length	45.0	m
Cylinder radius	3.25	m
Shell thickness	0.04	m
Stiffener cross-sectional area	0.012	m^2
Stiffener spacing	0.5	m
Young's modulus of structure without foundation	210	GPa
Young's modulus of foundation	200	GPa
Poisson's ratio of structure	0.3	
Density of structure	7800	kg/m^3
Structural loss factor	0.02	
Added mass	796	kg/m^2
Stern lumped mass (two-field problem)	188×10^3	kg
Stern lumped mass (three-field problem)	133×10^3	kg
Bow lumped mass	200×10^3	kg
Cone half angle	24	deg
Cone length	9.079	m
Cone smaller radius	0.3	m
Density of fluid	1000	kg/m^3
Speed of sound	1500	m/s

are shown in Fig. 10. The local peaks at 21 and 43 Hz are the first and second hull axial resonant frequencies. The RC reduces the maximum force transmissibility and detunes the fundamental resonant frequency of the propeller/shafting system from 37 to 12 Hz. In addition, the RC leads to a significant decrease of the force transmissibility above the fundamental resonant frequency. It is evident that the -180° phase shift due to the resonant frequency of the propeller/shafting system is not sustained in the case of the model with the RC, but reduces gradually to a -58° phase shift. This is assumed to play an important role for the combined dipole and

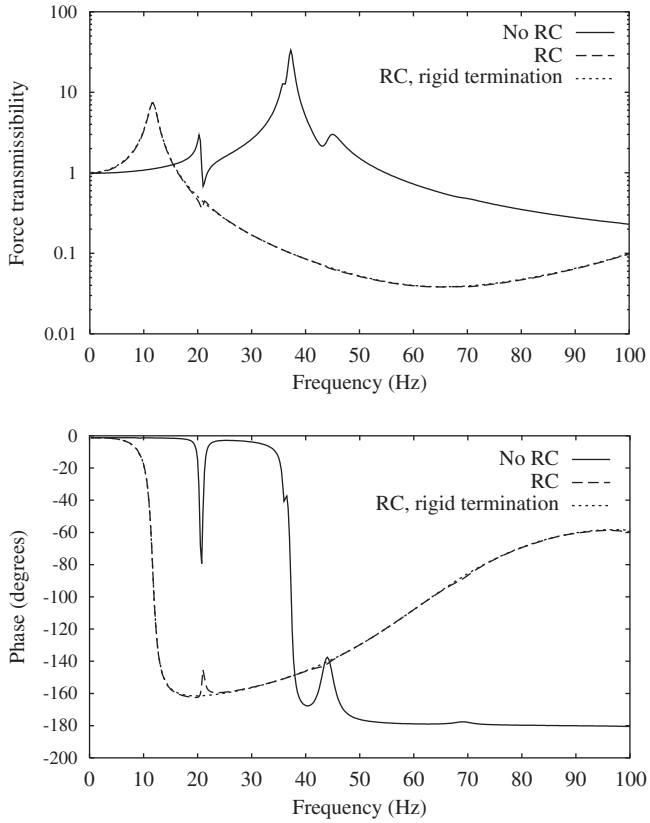

Fig. 10. Force transmissibility of the propeller/shafting system.

structural excitation, as cancellation or reinforcement effects may occur, depending on their relative phase. The difference between the model with a rigid termination and the model with the simplified physical model of the submarine are the local peaks at the hull resonant frequencies. Comparing the results with a rigid termination and a physical model of the hull shows that the effect of the drive point impedance on the force transmission is very small for the first hull axial resonant frequency (21 Hz) and negligible for the second and higher hull resonant frequencies. Clearly, the natural resonances of the submarine hull at 21 and 43 Hz have much less influence on the model with the RC, showing that the propeller/shafting system with the RC is less strongly coupled to the submarine hull.

The axial mobility of the propeller with and without the RC is shown in Fig. 11, where the simplified physical model of the submarine was considered as the termination. The maximum vibration of the propeller occurs at the fundamental resonant frequency of the propeller/shafting system, leading to increased sound radiation from the propeller.

5.2. *Influence of the tailcone properties on the structural and acoustic responses*

For structural and acoustic optimisation problems, computationally cost efficient models are required. However, for the free-flooded cone, a three-field problem is present rather than a two-field problem, leading to significantly larger and denser system matrices. An investigation of different tailcone models is therefore of interest. A first approximation to the tailcone is a rigid cone with no internal water, where the mass effect of the water is considered as a lumped mass at the pressure hull end plate in order to maintain the global dynamic behaviour of the hull. However, the stiffness of the tailcone has an influence on the sound radiation as well as the sensitivity of the structure to excitation from a nearby sound source. Therefore, additional models were

developed that represent a link between the model with internal fluid loading and the model with a rigid tailcone. The range of examined models includes:

(a) a flexible tailcone with internal water;
(b) a flexible tailcone with the same structural parameters as (a) but with a lumped mass representation of the internal water, where the lumped mass is attached to the rear end plate;
(c) a flexible tailcone with the lumped mass representation of the water as used for (b), but with an increased Young's modulus and
(d) a rigid tailcone with the lumped mass representation of the internal water as used for (b) and (c).

The mobility of the rear end plate is used to compare the models, where the exciting force is applied to (i) the rear end plate or (ii) the end of the tailcone. Results obtained using variation (i) allow assessment of the global behaviour of the model due to excitation via the shaft, whereas results obtained using variation (ii) are relevant for dipole excitation.

Fig. 12 shows the point mobility of the hull stern end plate. The lumped mass used to simulate the effect of the cone internal water was chosen such that the simplified model yields the best match with the model that includes internal water. The resonant frequencies and amplitude for the drive point mobility were chosen as the criteria for comparison of the models. A lumped mass that is about half the mass of the internal water was found to be the best approximation. In the case of the flexible cone without internal water, the stiffness was increased through the Young's modulus. The global behaviour of the structure is seen to be only

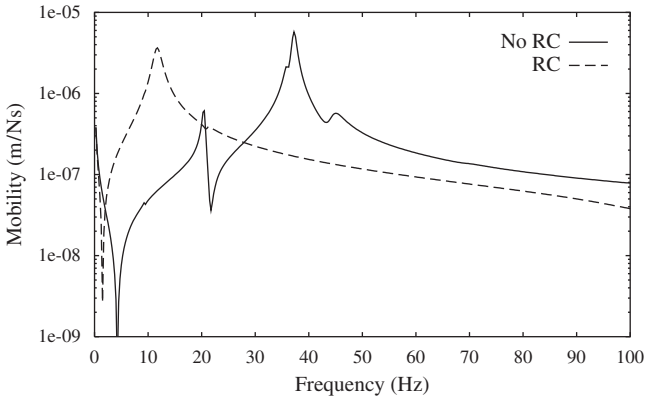

Fig. 11. Axial propeller mobility amplitude.

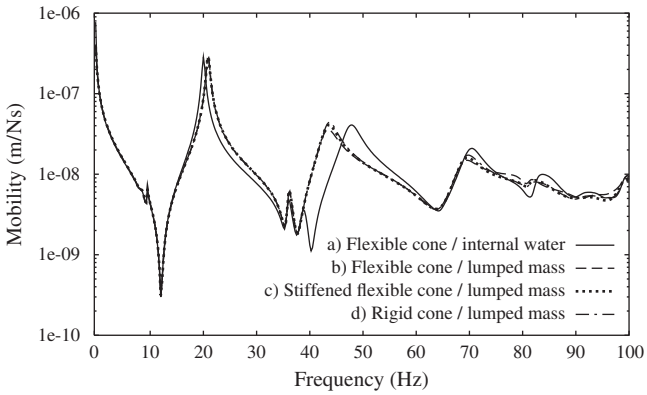

Fig. 12. Point mobility of the stern end plate using different representations of the free-flooded tailcone.

weakly dependent on assumptions about the tailcone properties for the models with no internal water. However, the structural mobility of the hull end plate changes for the model with internal water as local resonances of the cone occur within the investigated frequency range. The first four hull axial resonances can be identified at 21, 43, 70 and 99 Hz for models (b)–(d). For model (a), the first resonance of the cone at 39 Hz shifts the first resonance of the hull down by about 2 Hz and the second resonance up by about 4 Hz.

Fig. 13 shows the transfer mobility of the hull stern end plate for a structural force applied at the end of the tailcone. The results for models (a)–(d) now differ significantly for frequencies above 20 Hz. The results for models (b)–(d) diverge above about 43 Hz. It can be seen that an increase in flexibility leads to stronger responses for models (b)–(d). Using model (a), cone resonances also occur at 39, 64, 81 and 96 Hz. It can be concluded that the cone properties will not have a crucial impact on the structural response of the submarine hull for structural excitation. The structural response will, however, be underestimated for dipole excitation, where significant forces are applied near the end of the tailcone.

The influence of the assumed cone properties on radiated sound power is more significant, when the force is applied near the propeller end of the cone. Figs. 14 and 15 show the radiated sound power for the different representations of the cone, when the axial force is applied at the stern end plate and tailcone end, respectively. In Fig. 14, the results are all similar apart from the shift of the second hull axial resonant frequency. When the force is applied to the propeller end of the cone (Fig. 15), the assumed cone flexibility now has a significant influence on the radiated sound power at frequencies above about 25 Hz.

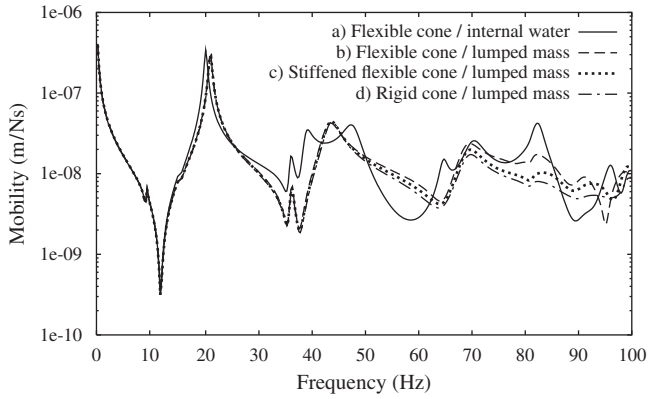

Fig. 13. Mobility of the stern end plate due to excitation of the tailcone end, using different representations of the free-flooded tailcone.

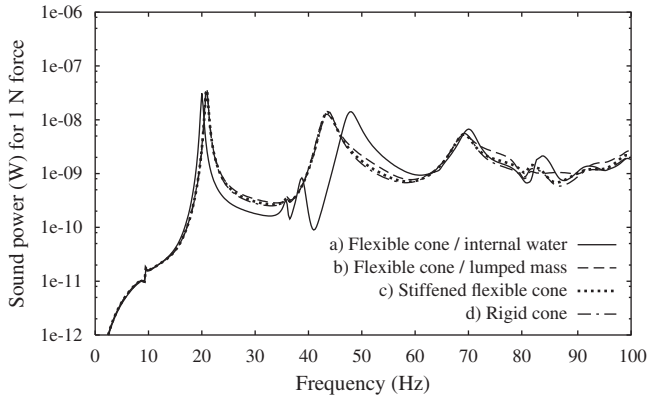

Fig. 14. Radiated sound power due to structural excitation of the stern end plate, using different representations of the free-flooded tailcone.

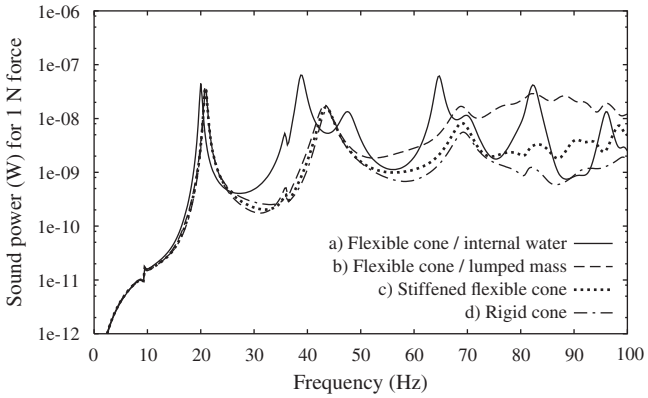

Fig. 15. Radiated sound power due to structural excitation of the tailcone end, using different representations of the free-flooded tailcone.

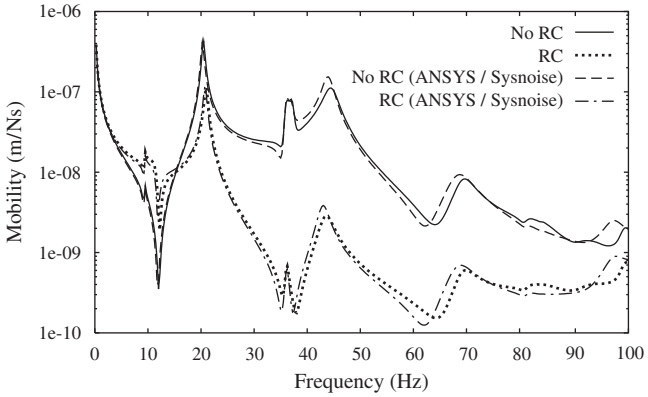

Fig. 16. Mobility of the stern end plate ignoring acoustic excitation.

The rigid cone has been used in the complete FE/BE model that includes the submarine hull as well as the propeller/propulsion system. However Fig. 15 shows that excitation due to the dipole is likely to be underestimated at frequencies above about 30 Hz, particularly at the cone resonances.

5.3. *Structural and acoustic responses for the coupled model under structural and acoustic excitation*

The structural and acoustic responses of the submarine hull have been investigated, where the tailcone was modelled as a rigid structure. Both structural excitation through the propeller/shafting system and acoustic excitation of the submarine hull have been considered. The acoustic excitation is due to dipole sound radiation caused by operation of the propeller in the non-uniform wake as well as propeller vibration. The acoustic response in the far field is a combination of sound radiated from the submarine hull due to structural and acoustic excitation and sound radiated directly from the propeller.

Fig. 16 shows the mobility of the hull stern end plate, due to structural excitation at the propeller hub. The broad peak near 37 Hz is due to a combination of the principal propeller/shafting system resonance and a bulkhead resonance. For validation, results are also presented for models where linear finite shell elements based on Kirchhoff–Love assumptions have been used for the structure [17]. Sysnoise was utilised to obtain the solution for the coupled model using boundary elements for the fluid. The frequencies are slightly shifted downwards for the models using Sysnoise. The reason is that the more accurate Reissner–Mindlin elements seem to be stiffer than the Kirchhoff–Love elements.

It is evident that vibration of the hull is significantly reduced by the RC for frequencies greater than 20 Hz. However, when considering acoustic excitation, the effect of the RC on end plate mobility is decreased, as shown in Fig. 17. The acoustic far field of the dipole plays an important role in the excitation of the submarine hull at higher frequencies, since the radius of transition from the near to the far field decreases with an increase of frequency.

To assess stealth, the overall radiated sound power including both sound radiation from the propeller and the submarine has been considered. The sound power was computed by integration of the intensity over a sphere of 1000 m radius with the centre on the axis of the submarine and 22.5 m forward in the axial direction from the stern end plate. For models with no dipole sources present, the sound power has been obtained by integration of the intensity over the submarine surface. Three cases have been examined. For each case, models with and without an RC have been investigated. For the first case, only structural excitation of the submarine hull through the propeller/shafting system has been considered. For the second case, excitation by the dipole field due directly to operation of the propeller in a non-uniform wake has been introduced. For the third case, structural excitation via the propeller shaft and excitation by both the dipole field due to operation of the propeller in a non-uniform wake and the dipole field caused by propeller vibration, have been taken into account. In the second and third cases, the direct radiated field from the propeller is also included in the computation of sound power.

Fig. 18 presents the results for the first case and shows that implementation of an RC in the propeller/shafting system leads to a significant reduction of overall radiated sound power. Results are also given for the

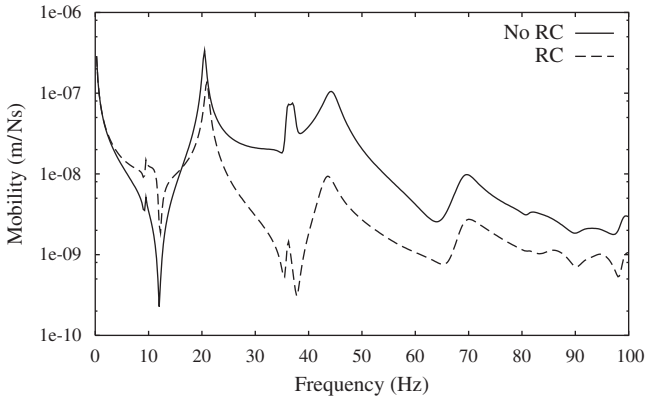

Fig. 17. Mobility of the stern end plate including acoustic excitation (dipole due to non-uniform wake and dipole due to propeller vibration).

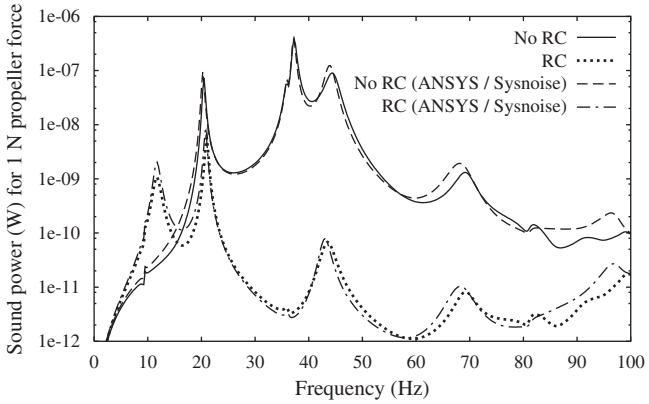

Fig. 18. Radiated sound power due to structural excitation.

model using linear finite elements and Sysnoise. As for the mobility prediction in Fig. 16, there are only small differences in the results from the two models. It can be seen that the peak at 37 Hz due to the fundamental resonance of the propeller/shafting system shifts to 12 Hz when an RC is implemented, leading to an increase in radiated sound power at lower frequencies. For the second case in Fig. 19, the sound radiation due to both structural and dipole excitation without the RC is greater than in Fig. 18, particularly at higher frequencies. This is attributed to excitation of the hull by the dipole field and the direct field from the propeller. Fig. 19 shows that excitation of the hull via the fluid has limited the effect of the RC to frequencies below about 75 Hz.

At very low frequencies, where the hull acts as a rigid body and the wavelength is very large, the radiated field due to the propeller dipole cancels that due to axial hull vibration; in effect, the force applied to the neutrally buoyant hull cancels the propeller dipole. This effect can be seen clearly below about 10 Hz in Fig. 19.

Fig. 20 shows the radiated sound power for the third case, where propeller vibration is taken into account. Implementation of an RC does not lead to a decrease of sound radiation at higher frequencies due to the dominance of dipole excitation. The two dipole fields change in relative magnitude and phase as frequency increases. At frequencies below the shaft resonant frequency, the dipole due to propeller vibration is weak. At frequencies below about 10 Hz the results shown in Figs. 19 and 20 are almost identical. At frequencies well above the shaft resonant frequency the dipoles partially cancel each other, so the predicted overall vibration is lower when propeller vibration is taken into account.

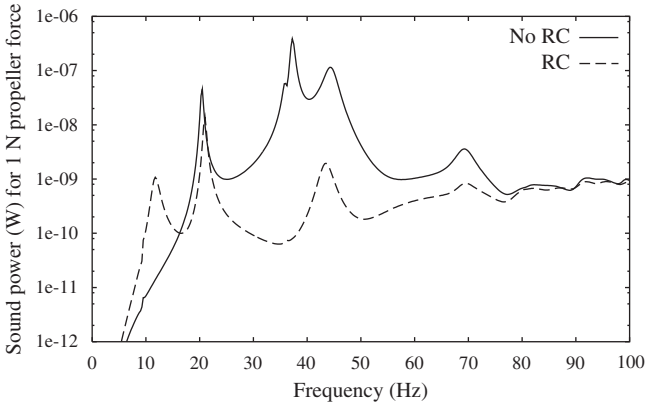

Fig. 19. Radiated sound power, where structural and acoustic excitation of the hull are considered. The dipole due to propeller vibration is not taken into account. The sound power is the combined effect of sound radiation due to hull vibration and direct sound radiation from the propeller.

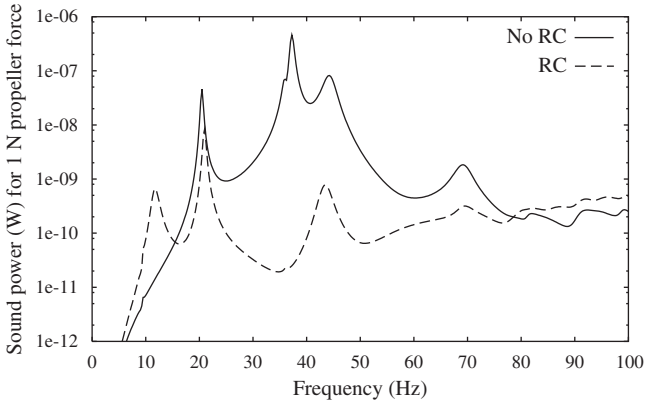

Fig. 20. Radiated sound power, where structural and acoustic excitation of the hull are considered. The acoustic excitation is due to the dipole caused directly by the operation of the propeller in a non-uniform wake and due to the dipole caused by propeller vibration. The sound power is the combined effect of sound radiation due to hull and propeller vibration and direct sound radiation from the propeller.

6. Conclusions

A numerical model has been developed to investigate the acoustic and structural responses of a submarine hull due to axial excitation from propeller forces. The propeller forces arise from a non-uniform wake and are transmitted to the hull via the fluid and the propeller/shafting system. The dynamic behaviour of the propeller/shafting system causes propeller vibration that generates additional sound radiation from the propeller. The tailcone of the submarine was represented as a rigid structure connected to the pressure hull. This was shown to be a reasonable approximation to a flexible free flooded cone at low frequencies, but the effects on overall sound radiation of forces transmitted through the fluid to the tailcone and hull structure are likely to be underestimated.

The efficiency of a vibration attenuation system known as a resonance changer in the propeller/shafting system has been examined. It was found that the performance of the RC is affected significantly by the influence of dipole fields due to hydrodynamic forces, which are always present, and propeller vibration. The two dipole fields may reinforce or partially cancel each other, depending on frequency and parameter selection. The RC can provide a significant reduction in overall radiated sound power at low frequencies, including propeller blade passing frequency, but will have a much more limited effect at higher frequencies where the dipole fields tend to be the dominant cause of radiated sound power.

In order to predict the overall sound radiation, acoustic excitation due to both dipole fields has to be taken into account. The resonant behaviour of the propeller blades should also be considered in a complete model. An optimal solution for the RC might then change the dynamic behaviour of the propeller/shafting system such that maximum advantage is taken of the interaction between propeller, shafting and hull dynamic characteristics.

References

[1] D. Ross, *Mechanics of Underwater Noise*, Penninsula Publishing, Los Altos, 1987.
[2] J.S. Carlton, *Marine Propellers and Propulsion*, Butterworth-Heinemann, Oxford, 1994.
[3] O. Rath Spivack, R. Kinns, N. Peake, Acoustic excitation of hull surfaces by propeller sources, *Journal of Marine Science and Technology* 9 (2004) 109–116.
[4] C.D. Bloor, A Study of the Acoustic Pressures on a Ship's Hull due to its Propellers, Ph.D. Thesis, University of Cambridge, 2001.
[5] P.G. Dylejko, Optimum Resonance Changer for Submerged Vessel Signature Reduction, Ph.D. Thesis, School of Mechanical and Manufacturing Engineering, University of New South Wales, 2008.
[6] Y.-Z. Kehr, J.-H. Kao, Numerical prediction of the blade rate noise induced by Marine propellers, *Journal of Ship Research* 48 (1) (2004) 1–14.
[7] J.P. Breslin, P. Anderson, *Hydrodynamics of Ship Propellers, Ocean Technology*, Cambridge University Press, Cambridge, 1994.
[8] O. Rath Spivack, R. Kinns, N. Peake, Hull excitation by fluctuating and rotating acoustics sources at the propeller, *Proceedings of the 25th Symposium on Naval Hydrodynamics*, St. John's, Newfoundland, Canada, 8–13 August 2004.
[9] H. Seol, B. Jung, J.-C. Suh, S. Lee, Prediction of non-cavitating underwater propeller noise, *Journal of Sound and Vibration* 257 (1) (2002) 131–156.
[10] C. Norwood, The free vibration behaviour of ring stiffened cylinders, Technical Report 200, DSTO Aeronautical and Maritime Research Laboratory, Melbourne, Australia, 1995.
[11] A.J.H. Goodwin, The design of a resonance changer to overcome excessive axial vibration of propeller shafting, *Institute of Marine Engineers—Transactions* 72 (1960) 37–63.
[12] P.G. Dylejko, N.J. Kessissoglou, Y.K. Tso, C.J. Norwood, Optimisation of a resonance changer to minimise the vibration transmission in marine vessels, *Journal of Sound and Vibration* 300 (2007) 101–116.
[13] G. Chertok, Forces on a submarine hull induced by the propeller, *Journal of Ship Research* 9 (2) (1965) 122–130.
[14] R. Kinns, I. Thompson, N.J. Kessissoglou, Y.K. Tso, Hull vibratory forces transmitted via the fluid and the shaft from a submarine propeller, *Ships and Offshore Structures* 2 (2) (2007) 183–189.
[15] S. Merz, N.J. Kessissoglou, R. Kinns, Excitation of a submarine hull by propeller forces, *Proceedings of the 14th International Congress on Sound and Vibration*, Cairns, Australia, 9–12 July 2007.
[16] X. Pan, Y. Tso, R. Juniper, Active control of radiated pressure of a submarine hull, *Journal of Sound and Vibration* 311 (2008) 224–242.
[17] O.C. Zienkiewicz, R.L. Taylor, The Finite Element Method: Its Basis and Fundamentals, sixth ed., Vol. 1, Elsevier, Butterworth-Heinemann, Amsterdam, London, 2005.
[18] K.-J. Bathe, *Finite Element Procedures in Engineering Analysis*, Prentice-Hall, Englewood Cliffs, NY, 1982.
[19] C.A. Brebbia, R.D. Ciskowski, *Boundary Element Methods in Acoustics*, Elsevier Applied Science, New York, 1991.

[20] Y.K. Tso, C.J. Jenkins, Low frequency hull radiation noise, Technical Report TR05660, Defence Science and Technology Laboratory (Dstl), UK, 2003.
[21] O.C. Zienkiewicz, R.L. Tayler, The Finite Element Method: Solid Mechanics, sixth ed., Vol. 2, Elsevier, Butterworth-Heinemann, Amsterdam, London, 2005.
[22] G. Kirchhoff, Zur Theorie der Lichtstrahlen, *Annalen der Physik* 254 (4) (1883) 663–695.
[23] T.W. Wu (Ed.), Boundary Element Acoustics, WIT Press, Southampton, 2000.
[24] A.F. Seybert, B. Soenarki, F.J. Rizzo, D.J. Shippy, A special integral equation formulation for acoustic radiation and scattering for axisymmetric bodies and boundary conditions, *Journal of the Acoustical Society of America* 80 (4) (1986) 1241–1247.
[25] D. Fritze, S. Marburg, H.-J. Hardtke, FEM–BEM-coupling and structural-acoustic sensitivity analysis for shell geometries, *Computers & Structures* 83 (2–3) (2005) 143–154.